Topic: PHC-11-2015:

Development of new diagnostic tools and technologies: in vivo medical imaging technologies

HYPMED

Digital Hybrid Breast PET/MRI for Enhanced Diagnosis of Breast Cancer

Grant Agreement Number: 667211

D 2.3 Quantitative Reconstruction Environment

|			
Lead Partner:	PHI		
Author(s):	André Salomon		
Work Package No:	2		
Estimated delivery date:	M32 (August 30, 2018)	**Actual delivery date:**	M78 (June 22, 2022)
Nature:	Demonstrator		
Dissemination level:	Public		

Table of Contents

Reconstruction Software

Technological overview

The reconstruction framework developed in Philips research is called "*PURE*" [1]. The two HYPMED rings will be reconstructed completely separately since no interactions between both rings are expected to provide useful additional information. In a first initial step, the list-mode input data is sorted according to the crystal indices and wrote as temporary list file in a modified format. Prior to each reconstruction, based on the detector geometry and the attenuation map, a sensitivity distribution is generated for subsequent use as correction factor matrix in an iterative ML-EM/OS-EM reconstruction. A basic flowchart of *PURE* can be found in Figure 1.
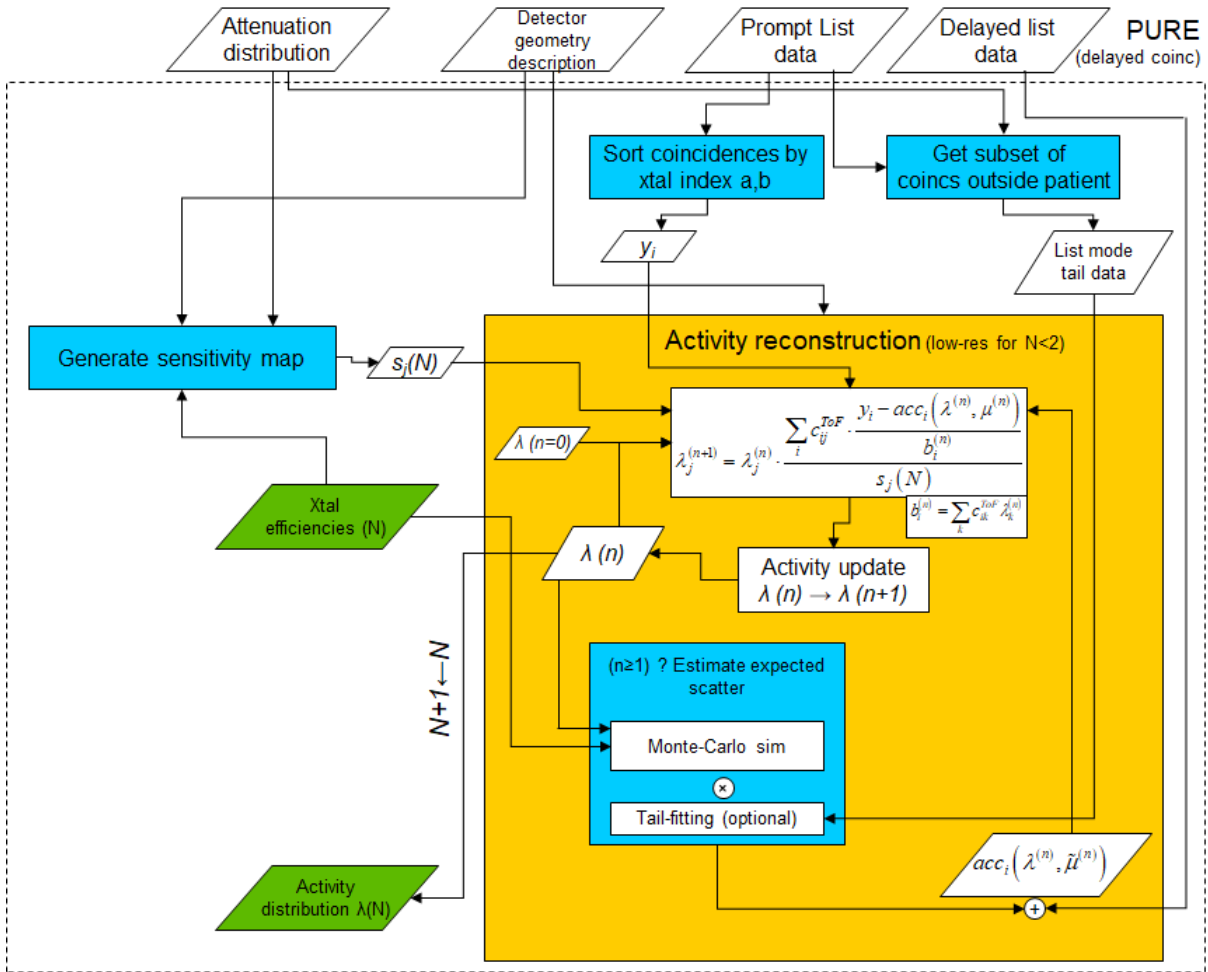
Figure 1: Reconstruction flowchart of voxel-based iterative reconstruction "PURE"

The core technology of this iterative reconstruction is the online processing of the system matrix entries modelling the tubes-of-responses (*TOR*s) for each coincidence (**Figure 2**, left and centre). The interaction of each *TOR* with the voxel-grid is estimated by a number of single lines-of-response (*LOR*s) (**Figure 2** and **Figure 3**, right). The voxel grid ray-tracing is realized using Siddon's algorithm [2]. In *PURE*, the start and end point of each line-of-response is randomly chosen inside the coincident crystals following an exponentially weighted probability distribution, which depends on the stopping power of the scintillation crystal material. Finally, the weights of all *LOR*s are summed up resulting in a list of voxel indexes and corresponding accumulated weights representing the *TOR*. Such list realizes the weighting values c_{ij} (see reconstruction formula in **Figure 1**) for a specific coincidence *j*.
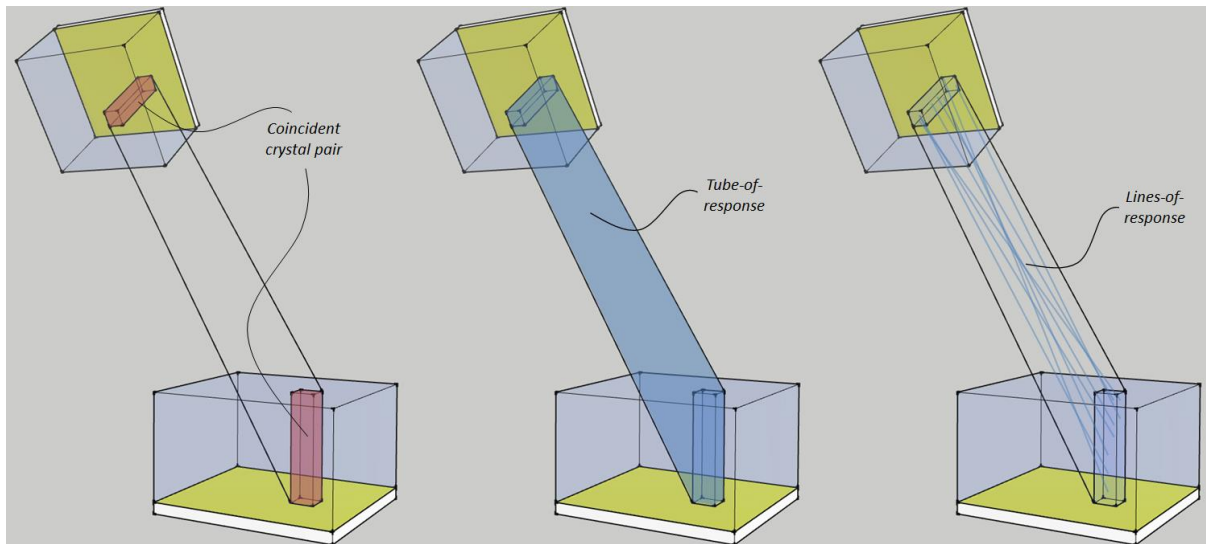
Figure 2: Left: coincident crystal pair in red, centre: corresponding TOR, right: corresponding single LORs with randomly chosen start and end points in the crystals
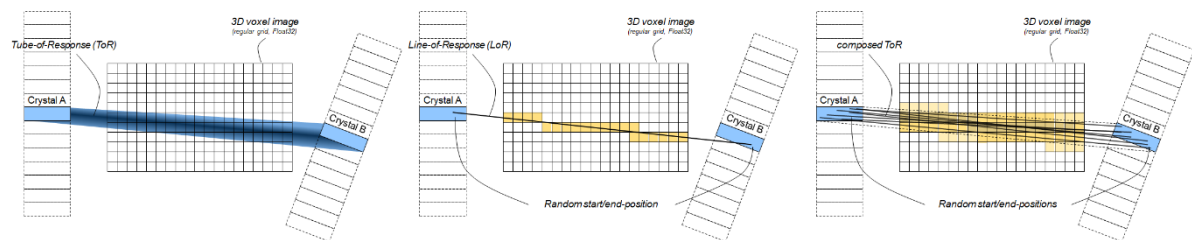

Figure 3: Left: ideal tube-of-response with spatially dependent probability distribution, centre: single LOR projected on voxel grid, right: multiple LORs with randomly chosen start and end points in the crystals projected on voxel grid

Accurate modelling of the *TOR* shape and spatial weighting provides an intrinsic resolution recovery effect in the forward- and back-projection. Typical values for the number of *LOR*s per *TOR* heavily depend on the ratio between the crystal size and the voxel size, since the estimated *TOR* should well represent the ideal *TOR* without introducing heavy Poisson noise or under-sampling artefacts in the emulated, projected *TOR*. Otherwise, the resolution recovery effect is affected, leading to a diminished spatial resolution in the reconstructed images.

In the used so-called list-mode reconstruction, each list-mode data entry is computed separately from all others, parallel on *N* cores using OpenMP (see also **Figure 4**):

1. Randomize start and end point of single LoR sample
   (iterative due to non-linear probability distribution)
2. Calculate list of voxel indices/weights and sums up image intensities along LoR
3. Repeat Steps 1. and 2. for remaining LoR samples and add all indices/weights to list; continue summing up image intensities along each LoR sample
4. Compute correction factor and backproject to image volume

Finally, the results of all *N* image volumes are merged and the result used to update the activity distribution estimate.
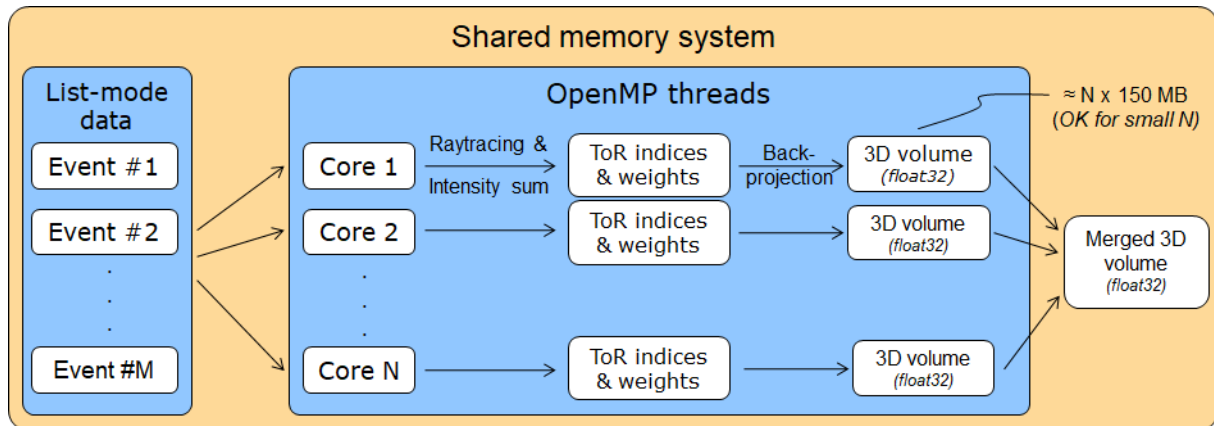
Figure 4: Parallel computing on shared memory system using OpenMP in PURE.

Corrections implemented in PURE

- Attenuation correction (based on μ-map)
- Crystal efficiencies (iteratively recovered using an activity source fully included by each of the two FOVs [3])
- Effective sensitivity (using geometrical configuration of the scintillator as visible in **Figure 5** as well as the μ-map and crystal efficiencies)
- Scatter correction (by subtraction of full Monte-Carlo simulated events using estimated activity distribution after each iteration)
- Random correction (by negative weighting of measured delayed coincidences, while prompt coincidence are positively weighted)
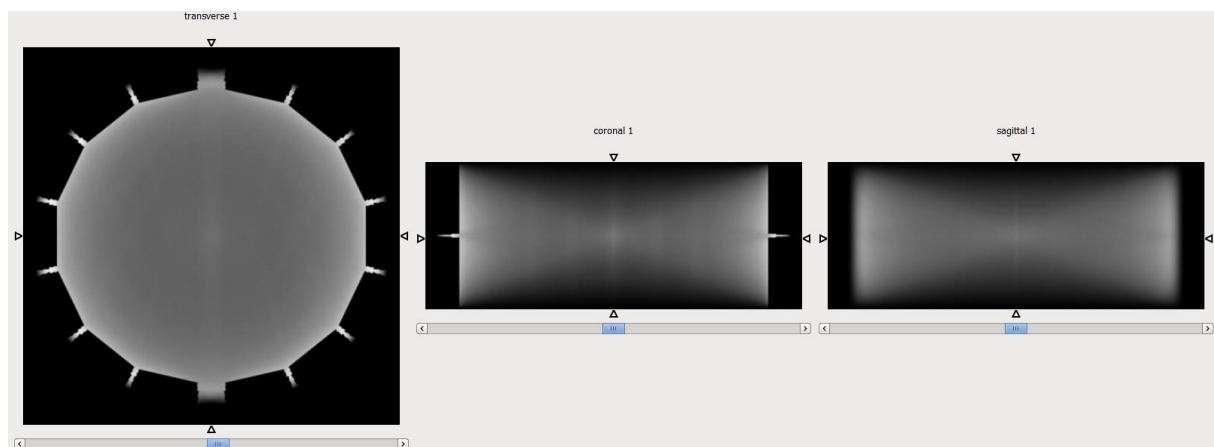
Figure 5: Estimated sensitivity distribution of an empty HYPMED ring (left: transverse, centre: coronal, right: sagittal) with an additional gap between the two half-rings of 2×7.486 mm.

Data format

The data format used for prompt and delayed coincidences looks for each coincidence event as described in Figure 6. For the HYPMED scanner, for each ring separately, each crystal DOI layer corresponds to one module while the stack index is always 0 (i.e., $Y\_a == Y\_b == 0$). This is because of the special non-regular shape of crystal stacks, which are composed of 3-4 DOI layers with unique dimensions, i.e., shape and number of crystals. Accordingly, the module index Z_a and Z_b is calculated by $Z = detectorID * numDOIlayers + DOIlayerID$ for the first (a) and second (b) event. The detectorID is calculated from the axial position pZ and the transverse position pX of the corresponding crystal stack as follows: $detectorID = pX * 2 + pZ$ according to 2 stacks per module (see also **Figure 7**).

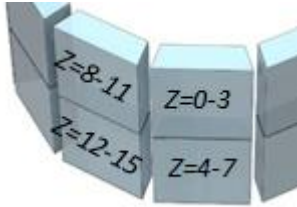|	Crystal index of event a,b		Stack index of event a,b		Module index of event a,b		(tStampB-tStampA) / ps	Framecounter
X_a	X_b	Y_a	Y_b	Z_a	Z_b	Δ_T	framecounter
Short16	Short16	Short16	Short16	Short16	Short16	Float32	Unsigned Int 64

Figure 6: List-mode data format

Figure 7: Z-indexing of crystal stack DOI layers (in case of 4 crystal DOI layers)

Recon tests with simulated data

In order to estimate the spatial resolution given a certain design and to test the reconstruction software, a simulation and reconstruction has been performed using the following steps (See also **Figure 8**):

1. Simulation of 2e8 coincidences for each proposed scanner design using an Archimedean spiral phantom which is covering the x–y plane, as well as the x–z and y–z plane of the PET FOV, i.e., three Archimedean spirals in a single phantom. Each spiral consists of spheres with 1mm diameter and 2 mm centre-to-centre distance.

2. Reconstruction of the simulated PET list-mode data and subsequent visual inspection – all single sources should be separable from each other.
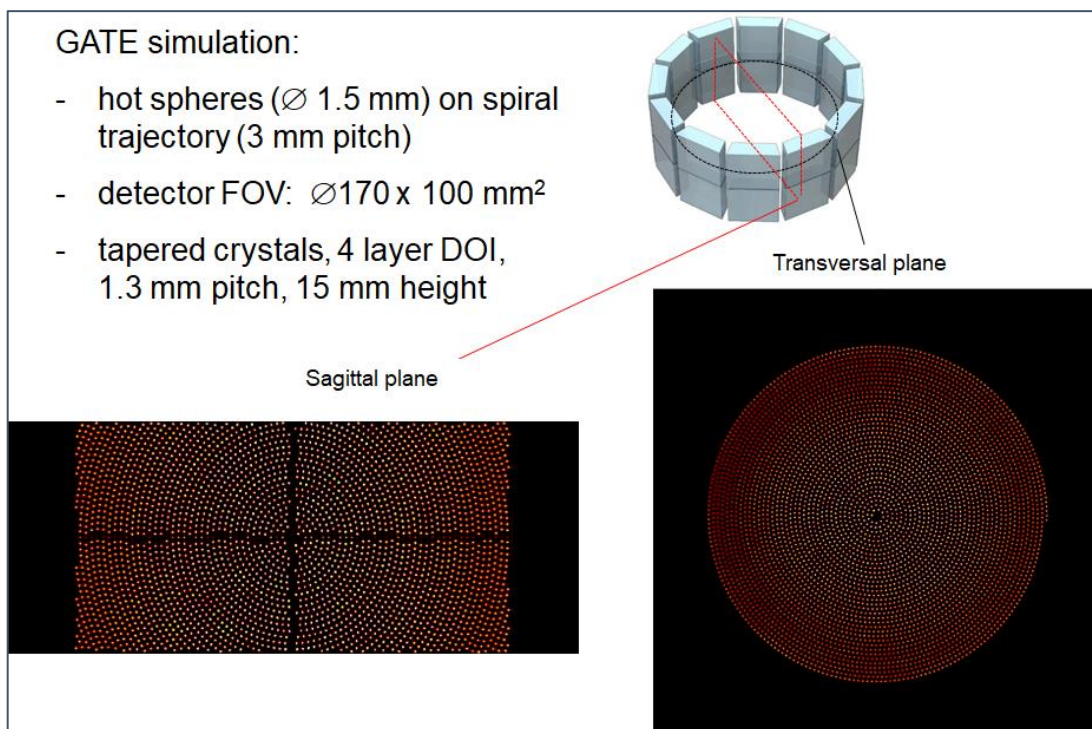

Figure 8: Reconstructed simulated list-mode data for investigating spatial resolution of the HYPMED PET device.

Reconstruction modes – real-time/offline reconstruction

*There are two modes in which the reconstruction can be used:*

1. Offline reconstruction:
   - Uses high quality correction methods for e.g., scatter and attenuation while needing significant computation effort (up to several hours depending on acquisition time and activated correction features)
   - High spatial resolution (~0.5-1 mm voxel size) with resolution recovery
   - OSEM or MLEM reconstruction available

2. Real-time reconstruction - must be supported by coincidence processing developed in WP1:
   - Uses low-resolution voxel size (i.e., 2–4 mm)
   - Processes image update (i.e., OSEM subset) after each 500k–1M measured coincidences
   - Sufficiently fast for generating intermediate images during PET acquisition

Recon tests with measured data

Point-source measurements with a single detector ring have been reconstructed. For debugging purposes, the planar projection of the corresponding sinogram (see **Figure 9**), as well as a simple back projection of measured coincidences (see **Figure 10**) have been generated. For the reconstruction volume, a voxel pitch of 1 mm has been used and a total of 288×288×98 voxels in x,y,z-dimension. For the reconstructed image in **Figure 11**, 32 iterations of MLEM have been used.
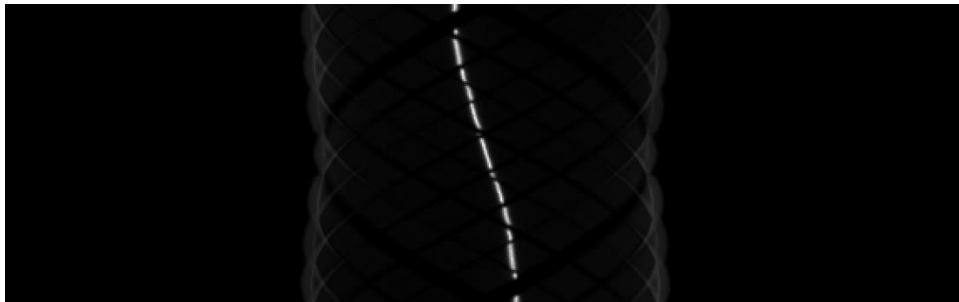
**Figure 9**: Planar projection of rebinned measured sinogram

Coronal

Sagittal
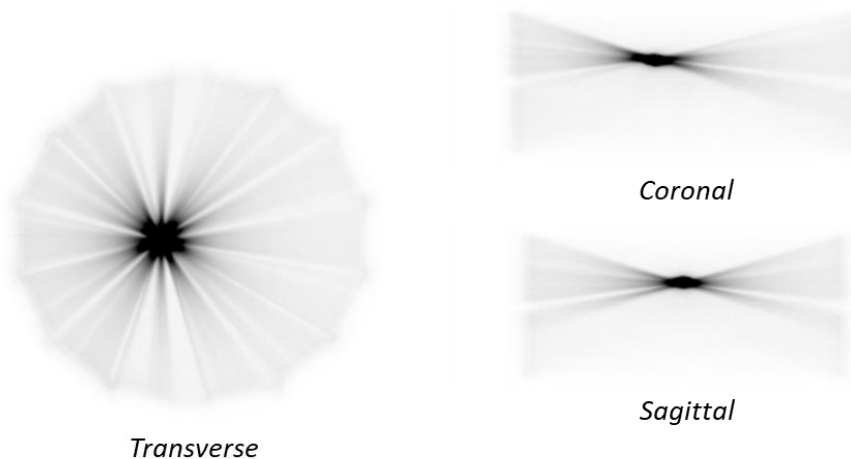
Transverse

Figure 10: Back-projected measured coincidences in transverse, coronal, and sagittal view centred on the point source

Figure 11: Focused reconstructed point source in transverse, coronal and sagittal slice view

Both the projected sinogram in **Figure 9** and the back-projection image in **Figure 10** do not show unexpected artifacts, i.e., other than the expected missing observation angles due to the gaps between adjacent detector stacks.

Equivalent investigations have been done for phantom measurements with FDG such as with a structured phantom as shown in **Figure 12** and a cylindrical phantom.
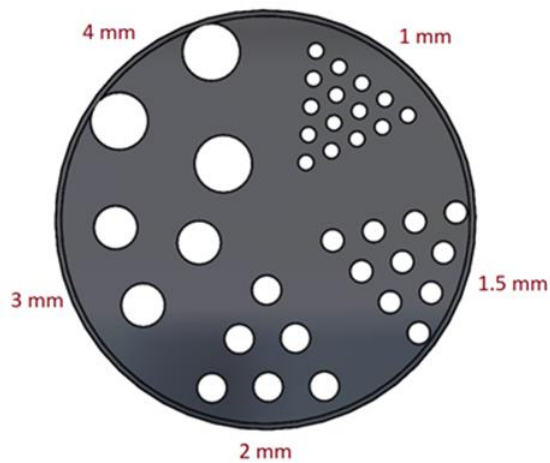
Figure 12: Structured phantom measured at UKA
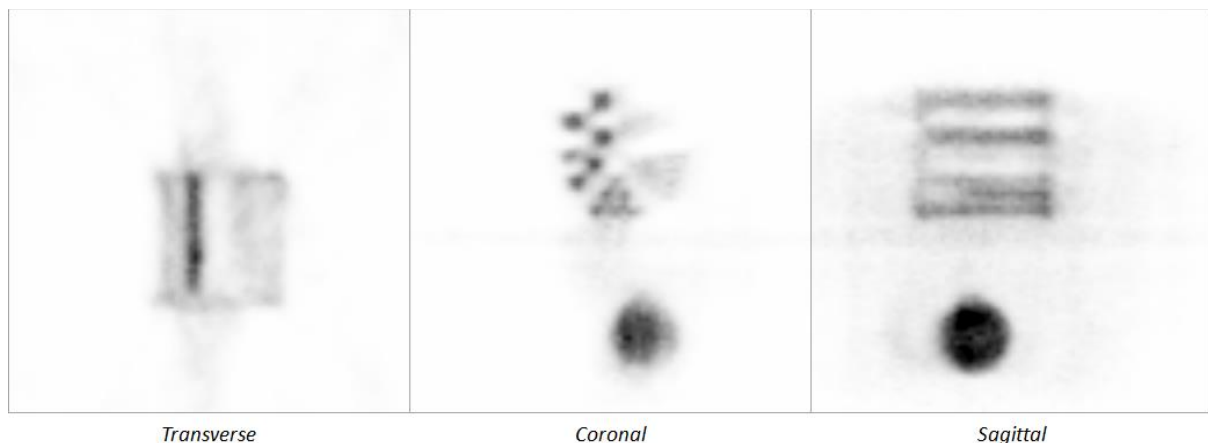
Figure 13: Reconstructed PET image of a simultaneous PET/MR acquisition of a structured phantom and homogenous cylindrical phantom filled with FDG.

Reconstruction of correspondent measured data from a simultaneous PET/MR acquisition is shown in **Figure 13**. First assessment of the spatial PET resolution with the current acquisition software is between 1.5 mm and 2 mm.

Conclusions

First tests with measured data have shown that the reconstruction software is capable of reconstructing data from the HYPMED scanner. We are therefore looking forward to measuring more complex phantom and clinical data which will also provide attenuation maps for scatter and attenuation correction, as well as random correction that becomes relevant for significant out-of-FOV activity. Currently achieved spatial resolutions of <2 mm will be further improved by future version of the singles processing and corresponding crystal identification software addressed in WP1.

References

[1] A. Salomon, A. Goedicke, B. Schweizer, T. Aach, V. Schulz, "Simultaneous reconstruction of activity and attenuation for *PET*/MR", IEEE Trans. Med. Imaging., vol. (3), 804-813, 2011

[2] Siddon RL, "Fast calculation of the exact radiological path for a three-dimensional CT array", Med. Phys., vol. 12(2), pp. 252-255, 1985

[3] A. Salomon, B. Goldschmidt, R. Botnar, F. Kiessling, V. Schulz, „A self-normalization reconstruction technique for PET scans using the positron emission data", IEEE Trans Med Imag, 2012